



HAL
open science

On the O-rich domain of the U-Am-O phase diagram

E. Epifano, Romain Vauchy, Florent Lebreton, R. Lauwerier, A. Joly, Andreas C. Scheinost, C. Guéneau, Ch Valot, P.M. Martin

► To cite this version:

E. Epifano, Romain Vauchy, Florent Lebreton, R. Lauwerier, A. Joly, et al.. On the O-rich domain of the U-Am-O phase diagram. *Journal of Nuclear Materials*, 2020, 531, pp.151986. 10.1016/j.jnucmat.2020.151986 . cea-02529003

HAL Id: cea-02529003

<https://cea.hal.science/cea-02529003>

Submitted on 7 Mar 2022

HAL is a multi-disciplinary open access archive for the deposit and dissemination of scientific research documents, whether they are published or not. The documents may come from teaching and research institutions in France or abroad, or from public or private research centers.

L'archive ouverte pluridisciplinaire **HAL**, est destinée au dépôt et à la diffusion de documents scientifiques de niveau recherche, publiés ou non, émanant des établissements d'enseignement et de recherche français ou étrangers, des laboratoires publics ou privés.



Distributed under a Creative Commons Attribution - NonCommercial 4.0 International License

On the O-rich domain of the U-Am-O phase diagram

E. Epifano,[†] R. Vauchy,[†] F. Lebreton,[†] R. Lauwerier,[†] A. Joly,[†] A. Scheinost,[‡] C. Guéneau,[¶] Ch. Valot,[†] and P. M. Martin^{*,†}

[†]*CEA, Nuclear Energy Division, Research Department on Mining and Fuel Recycling Processes, SFMA, BP 17171, F-30207 Bagnols sur Cèze, France*

[‡]*The Rossendorf Beamline at ESRF, Grenoble, France, and Institute of Resource Ecology, HZDR, Dresden, Germany.*

[¶]*DEN-Service de Corrosion et du Comportement des Matériaux dans leur Environnement (SCCME), CEA, Université Paris-Saclay, F-91191 Gif-sur-Yvette, France*

E-mail: enrica.epifano@onera.fr

Abstract

Uranium-Americium oxides $U_{1-y}Am_yO_{2\pm x}$ are promising candidates as possible transmutation targets for next generation nuclear reactors. In the context of a comprehensive investigation of their thermodynamic and thermal properties, the behaviour in oxidizing conditions is here studied. In a recent work, the behaviour in air of stoichiometric and sub-stoichiometric $U_{1-y}Am_yO_{2-x}$ compounds, with various Am content, was investigated by high-temperature X-ray Diffraction. Herein, the hyper-stoichiometric oxides obtained from that study are investigated by X-ray Absorption Spectroscopy. The new data, together with the previous XRD results, allow determining the exact compositions of the samples and hence obtaining phase diagram points in the O-rich domain of the U-Am-O system. **Indeed, five phase diagram points at 1473 K are obtained: two**

tie-lines in the M_4O_9 - M_3O_8 domain, for $Am/(Am+U)=0.10$ and 0.15 , one tie line in the MO_{2+x} - M_3O_8 domain, for $Am/(Am+U) = 0.28$, and two points in the single phase $MO_{2\pm x}$ domain, for higher americium concentration. From these data, it is also concluded that trivalent americium has a small solubility in the M_4O_9 and M_3O_8 phases.

1 Introduction

Uranium-ameridium mixed dioxide $U_{1-y}Am_yO_{2\pm x}$ are promising materials as transmutation targets for generation IV nuclear reactors.¹ To prevent the corrosion of the cladding, one of the requirements of the fuel design is that the dioxides must be oxygen deficient, i.e. oxygen/metal ratio (O/M) ≤ 2.0 . It is hence not surprising that the first investigations on the U-Am-O system focused on the oxygen hypo-stoichiometric domain.²⁻⁸ However, in order to assure the safety of reactors both in normal and accidental conditions, a comprehensive knowledge of the thermal and thermodynamic properties of the materials present in the reactor is necessary. Very few data exist on the O-rich domain of the U-Am-O phase diagram. The data are limited to some melting temperatures measured in air,⁹ a TGA oxidation of a mixed oxide with $Am/M = 0.80$,¹⁰ the oxygen potentials of $U_{0.50}Am_{0.50}O_{2+x}$ ¹¹ and a study indicating a small solubility ($Am/M = 10$ at.%) of americium in the hexagonal α' - M_3O_8 structure (s.g. P-62m).¹² In this work, the MO_{2+x} - M_4O_9 - M_3O_8 phase equilibria are issued. In the first part, the behaviour of $U_{1-y}Am_yO_{2\pm x}$ with $0.10 \leq y \leq 0.67$, in air, from room temperature up to 1473 K, was investigated by High-Temperature X-ray Diffraction (HT-XRD).¹³ It has been shown that the addition of americium to the dioxide hindered the formation of higher oxides, such as M_3O_8 . Indeed, by increasing the americium content, the appearance of this phase is delayed to higher temperatures, while the total amount diminishes. For an oxide with $Am/(Am+U) = 0.28$, only 5 wt.% of M_3O_8 was formed after a thermal treatment of 4 hours at 1473 K, while oxides with $Am = 0.48$ and 0.67 remained single-phase fluorites.

In this second part, the samples previously oxidized during the HT-XRD experiments are characterized by X-ray Absorption Spectroscopy (XAS). This technique has proven to be very useful to investigate the electronic properties and the local structure features of actinide oxides.^{3,5,8} Besides, in these mostly ionic materials, the oxidation states of the cations is directly related to the oxygen amount (electroneutrality). Therefore, in this study, the O/M ratio of the oxidized compounds will be determined and this will allow obtaining phase diagram data in the O-rich domain of the U-Am-O phase diagram at 1473 K.

2 Experiment

2.1 Materials

The precursor materials and the synthesis process for the $U_{1-y}Am_yO_{2\pm x}$ pellets with nominal $y = 0.10, 0.15, 0.30, 0.50$ and 0.70 was described in detail in a previous work.¹³ The UMACS process¹⁴ was used for the synthesis and the obtained samples had properties comparable with those of previous studies.^{15,16} The pellets were ground in an agate mortar and the obtained powder samples were annealed in a HT-XRD under flowing purified air. All the studied compositions underwent the same thermal treatment under air. They were heated from room temperature up to 1473 ± 15 K, with temperature steps of 50 K. At each step, a 30 minutes plateau was performed (time necessary for the acquisition of a diffraction pattern). The heating rate between the steps was 5 K/s. At the end of the heating stage, a plateau of 4 hours was performed at the maximum temperature. XRD patterns were acquired during this dwell time and no evolution was observed, indicating that the equilibrium was likely reached. Finally, the samples were cooled down recording a diffraction pattern every 100 K. A cooling rate of 5 K/s was applied between the steps. The lattice parameters of the cubic structures (MO_2 or M_4O_9 , depending on the sample) exhibited a regular, linear decrease, without any discontinuities (see Annex). For this reason, it is supposed that the cooling was fast enough to maintain the composition reached at 1473 K. The Rietveld refinement of the

XRD patterns acquired at room temperature allowed determining the phase compositions of the samples. These are summarized in Table 1.

Table 1: Compositions of the investigated samples. The Am/(Am+U) ratio was measured by TIMS (Thermal Ionization Mass Spectrometry). The phase repartition was determined by Rietveld refinements of the XRD patterns acquired at room temperature after oxidation.

Sample	Am/(Am+U) (at.%)	MO _{2+x} (wt.%)	M ₄ O ₉ (wt.%)	M ₃ O ₈ (wt.%)	R _{wp} (%)
Am10ox	10	-	21(5)	79(5)	9.5
Am15ox	15	-	43(5)	57(5)	7.6
Am30ox	28	95(5)	-	5(4)	5.3
Am50ox	48	100	-	-	5.1
Am70ox	67	100	-	-	5.4

The XAS study was performed at the ROBL beamline of the ESRF (Grenoble, France), 4 months after the HT-XRD measurements. During that period, the samples were stored in glove boxes in an inert N₂ atmosphere.

2.2 Experimental set-up

The XAS spectra were recorded at the ROBL beam-line at the ESRF (Grenoble, France) under dedicated operating conditions (6.0 GeV, 180 mA). Measurements were performed at room temperature and at 15 K, using for the latter a closed-cycle helium cryostat. Spectra were collected at the Am-L₃ (18510 eV), U-L₃ (17166 eV) and U-L₂ (20948 eV) edges in both transmission and fluorescence modes, using ionization chambers filled with N₂/Ar and a Canberra energy-dispersive 13-element germanium solid state detector. A double Si(111) crystal monochromator was used for energy selection and the calibration was performed using metallic foils, namely yttrium (17038 eV), zirconium (17998 eV), and molybdenum (20000 eV). The references were measured at the same time as the samples, in transmission mode, using a third ionization chamber behind the foil. The XANES spectra have been normalized using linear functions for pre- and post-edge modelling. The white-line maxima have been determined as the first zero-crossing of the first derivative. Pre-edge removal, normalization and self-absorption correction were performed using the ATHENA software.¹⁷ Standard

materials with known oxidation states were adopted for the analysis of the XANES data: an Am^{3+} -oxalate¹⁸ and Am^{4+}O_2 for americium,¹⁹ U^{4+}O_2 , $(\text{U}_{0.5}^{4+}, \text{U}_{0.5}^{5+})_4\text{O}_9$ and $(\text{U}_{2/3}^{5+}, \text{U}_{1/3}^{6+})_3\text{O}_8$.²⁰ The XANES spectra of the oxidized compounds were fitted by linear combination of the standards, in the energy range $E_{wl} - 20\text{eV} \leq E \leq E_{wl} + 20\text{eV}$, with E_{wl} being the white line energy. From these fits, the average oxidation states of the cations were obtained.

The EXAFS oscillations were extracted from the raw data with the ATHENA software¹⁷ and Fourier-transformed using a Hanning window. For the *Am50ox* sample, the EXAFS data were fitted using a structural model. In this case, interatomic scattering path phases and amplitudes were calculated with the FEFF 8.40 *ab initio* code.²¹ The ARTEMIS software was used for curve fitting in k^3 . For the other samples, presenting two phases, the EXAFS data were fitted by linear combination of the standards.

3 Results

3.1 Cationic charges and O/M ratios by XANES

The XANES spectra collected at the L_3 edge of Am and U and their corresponding second-derivatives are shown in Fig. 1 and Fig. 2, respectively. The spectra are compared to standard compounds and to the as-manufactured samples, i.e. before oxidation, for which a previous study was presented in.⁸ For simplicity, the nomenclature "AmY" and "AmYox", with Y equal to the (nominal) overall $\text{Am}/(\text{Am}+\text{U})$ ratio, is here adopted, for the oxides before and after treatment in air, respectively.

For *Am70ox*, a problem occurred during the recovering of the powder from the HT-XRD set-up or the preparation for the synchrotron (at room temperature). A high quantity of Pu was found by XAS in the sample (absent in the as-sintered oxide), probably from a contamination with a (U,Pu) O_2 oxide (stored in the same glove boxes). As a consequence, the spectra collected at the U edges cannot be considered representative of the oxidized $\text{U}_{0.33}\text{Am}_{0.67}\text{O}_{2\pm x}$ sample and they are not reported. Only the Am- L_3 edge is thus reported,

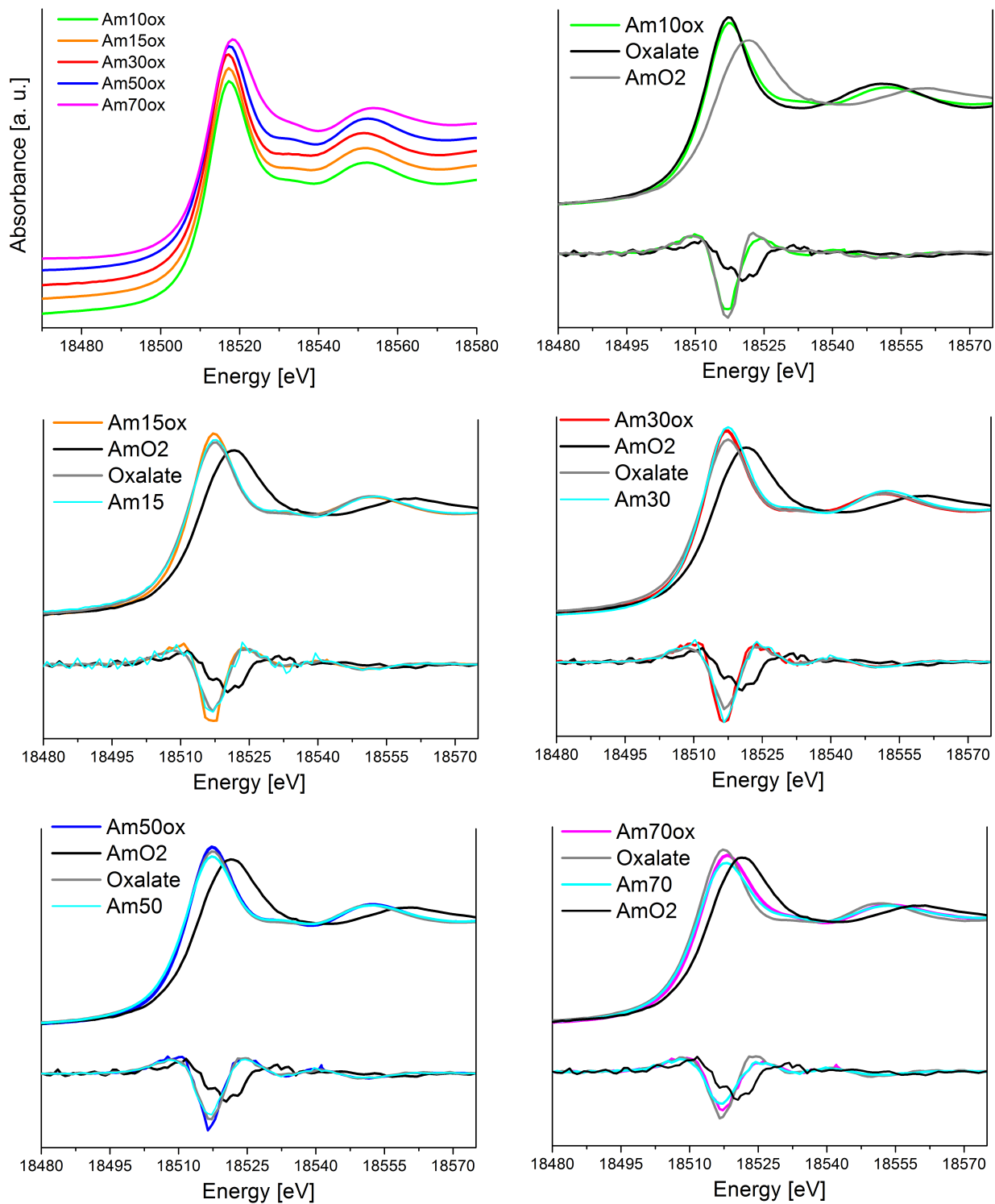


Figure 1: XANES spectra collected at the L₃ edge of Am and their second derivatives for the (U,Am)O₂ samples before and after oxidation in air.

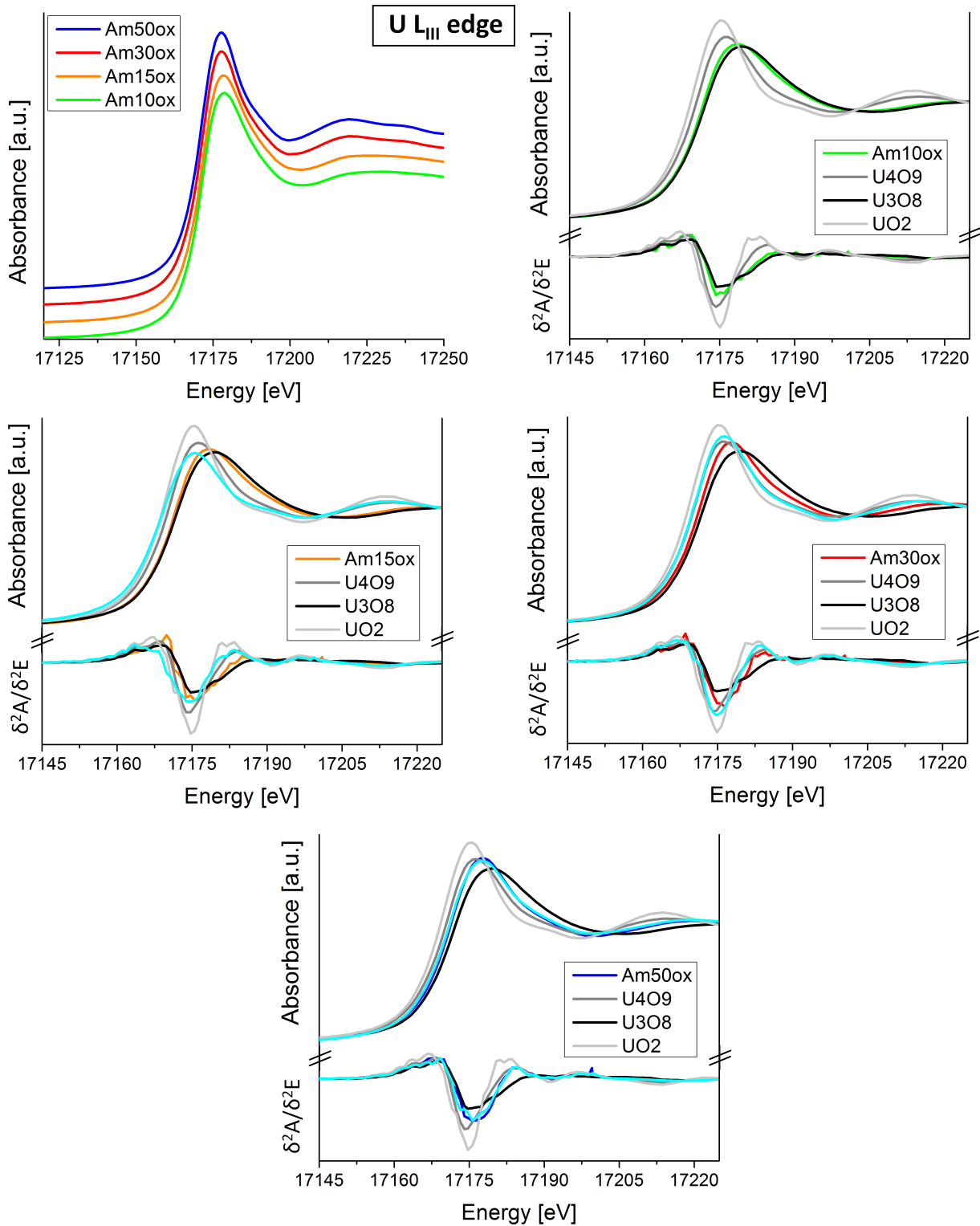


Figure 2: XANES spectra collected at the L_3 edge of U and their second derivatives for the $(U,Am)O_2$ samples before (light blue) and after oxidation in air.

in the hypothesis that the MOX contamination did not affect the americium chemical state in the (U,Am)O₂ dioxide. The observed energies of the inflection points and the white lines are compared in Tab. 2.

For the Am L₃ edge, the inflection points and the white line positions of all the oxidized

Table 2: Energy positions of the inflection points and white lines of the XANES spectra presented in Fig. 1 and Fig. 2. Values are given with a 0.2 eV standard uncertainty.

Sample	Am L ₃ edge [eV]		U L ₃ edge [eV]	
	Inflection point	White line	Inflection point	White line
Am10ox	18512.9	18517.4	17171.7	17178.7
Am15	18512.8	18517.3	17169.0	17175.4
Am15ox	18512.5	18517.4	17171.3	17178.4
Am30	18512.7	18517.4	17171.6	17176.4
Am30ox	18512.8	18517.1	17171.7	17177.8
Am50	18512.5	18517.4	17171.6	17177.7
Am50ox	18512.5	18517.4	17171.3	17177.9
Am70	18513.0	18518.0	17171.2	17177.9
Am70ox	18513.1	18518.3	-	-
Oxalate [Am ³⁺]	18513.0	18517.3	-	-
AmO ₂	18514.5	18521.5	-	-
UO ₂	-	-	17170.2	17175.4
U ₄ O ₉	-	-	17170.9	17176.3
U ₃ O ₈	-	-	17171.9	17179.6

samples are identical, within the experimental uncertainty, to the as-manufactured oxides. These energies are very close to the Am³⁺-oxalate reference, whereas the AmO₂ white line is shifted to higher energy of more than 3 eV. This indicates that americium is prevalently trivalent in the mixed oxides. It can seem surprising that americium is in the trivalent state in oxides annealed in air, but this is consistent with several previous investigations.^{3-5,8} Indeed, in uranium-amerium mixed oxides, americium is very stable in the trivalent state, when uranium is partially oxidized to the pentavalent state. Only for Am/(Am+U) > 0.50, tetravalent americium has been observed.⁸ Indeed, in agreement with the previous results, a slight shift toward higher energies is observed for the *Am70ox* sample, due to the mixed Am³⁺/Am⁴⁺ oxidation state.⁸ The corresponding oxidized sample presents a very similar

white line position, only slightly shifted toward higher energies, likely indicating a further small increase in the Am^{4+} fraction.

The spectra collected at the U-L₃ edge show remarkable differences between the as-sintered and oxidized samples, being generally shifted toward higher energies. For the *Am10ox*, *Am15ox*, *Am30ox* samples, the white line positions are between those of the U₄O₉ and the U₃O₈ references, indicating a high average oxidation state of uranium. This is consistent with the presence of the cubic and the M₃O₈ phases in these samples, revealed by the HT-XRD results. For the $\text{Am}/(\text{Am}+\text{U}) = 0.5$ composition, the white line position is found at slightly higher energies than that of U₄O₉ reference, similarly to the as-sintered oxide. A quantitative determination of the U and Am oxidation states was performed by fitting the U-L₃ and Am-L₃ XANES spectra as a linear combination of the standard compounds. The results of the fits for the oxidized samples are provided in Tab. 3. A generally good agreement between the data and the fit was achieved, as indicated by the low R-factor of the fits.

Table 3: Results of the linear combination fit of the U-L₃ and Am-L₃ XANES spectra using the reference compounds: fraction of the combinations, R-factor of the fit, average oxidation state (AOS) and O/M ratio computed from the oxidation states.

Sample	Am L ₃ edge				U L ₃ edge				Overall O/M	
	Am ³⁺	AmO ₂	R-factor	AOS	UO ₂	U ₄ O ₉	U ₃ O ₈	R-factor		AOS
Am10ox	1	0	0.001	3	0	0.20	0.80	0.001	5.17	2.48(2)
Am15ox	1	0	0.001	3	0	0.25	0.75	0.001	5.13	2.40(2)
Am30ox	1	0	0.002	3	0	0.46	0.54	0.002	4.95	2.20(2)
Am50ox	1	0	0.002	3	0	0.54	0.46	0.002	4.88	1.99(2)
Am70ox	0.67	0.32	0.002	3.32	-	-	-	-	4.89	≥ 1.91

For the Am L₃ edge, the fit confirmed the presence of americium exclusively in the trivalent state for the oxidized samples with $\text{Am}/(\text{Am}+\text{U}) \leq 0.48$. The *Am70ox* sample presents a mixed $\text{Am}^{3+}/\text{Am}^{4+}$ composition, with an average oxidation state of +3.32(3), slightly

higher than that of the as-sintered oxide, equal to $+3.26(3)$.⁸

For the U L_3 edge, the best fits were obtained using the U_4O_9 and U_3O_8 references. For the *Am10ox*, *Am15ox* and *Am30ox* samples, the high average oxidation states, ranging from $+4.95$ to $+5.17$, are due to the presence of uranium in both the cubic and the M_3O_8 phases. For the *Am50ox* sample, constituted by a single cubic phase, the average oxidation state of uranium was equal to $+4.88(3)$, slightly higher than that of the as-sintered oxide ($+4.82^8$), but still lower than $+5$. Therefore, a U^{4+}/U^{5+} mixture can be supposed, since the presence of hexavalent uranium can be excluded, as shown by Epifano *et al.*⁸ As already said, for the *Am70ox*, the data relative to the U-edge are not reported because the sample was contaminated by MOX during the preparation and hence the results on this edge are not reliable.

The overall O/M_{tot} ratios of the samples were computed, from the knowledge of the average oxidation states of Am and U (the measured Am/M ratios of Table 1 were used for the calculations, instead of the nominal ones). For the biphasic samples, the O/M ratio of the cubic phase (O/M_{cubic}) was hence derived from the balance relation:

$$O/M_{tot} = a \cdot O/M_{cubic} + b \cdot 2.667, \quad (1)$$

where a and b are the molar fraction of the cubic and the M_3O_8 phase, respectively, which were derived by the Rietveld XRD refinements (Table 1). In Eq. (1), the M_3O_8 is supposed to be a stoichiometric compound ($O/M = 2.667$). The resulting compositions of the oxidized samples are summarized in Tab. 4 and represented in Fig. 3. For the U cationic fractions, the presence of U^{6+} in the cubic phase was excluded, on the basis of the results presented in.⁸ For the (MOX-contaminated) *Am70ox* sample, the data collected on the Am-edge are used, in the hypothesis that the MOX contamination does not affect the americium in the sample (this is likely since, as said before, the contamination occurred after the oxidation,

Table 4: Compositions of the cubic phase of the oxidized samples. *a*: not available data, supposed from the as-sintered oxide.

Sample	Overall composition			Cubic phase composition				
	Cubic[mol.%]	M ₃ O ₈ [mol.%]	O/M _{tot}	Am ³⁺	Am ⁴⁺	U ⁴⁺	U ⁵⁺	O/M
Am10ox	0.45(5)	0.55(5)	2.48(2)	0.10	0	0.3	0.60	2.25(5)
Am15ox	0.70(5)	0.30(5)	2.40(2)	0.15	0	0.13	0.72	2.28(5)
Am30ox	0.98(4)	0.02(4)	2.20(2)	0.28	0	0.05	0.67	2.19(5)
Am50ox	1	0	1.99(2)	0.48	0	0.06	0.46	1.99(2)
Am70ox	1	0	1.91(2)	0.46	0.21	0.26 ^a	0.28 ^a	1.91(2) ^a

at room temperature). For uranium, since the XANES spectra could not be collected (MOX presence clearly alter the uranium edge), the data of the as-sintered sample were adopted. The *real* O/M ratio is expected to be equal or higher than the calculated value of 1.91(2). Indeed, a reduction of uranium during the heating in air would be very unlikely and hence the O/M ratio cannot be lower than the value here proposed.

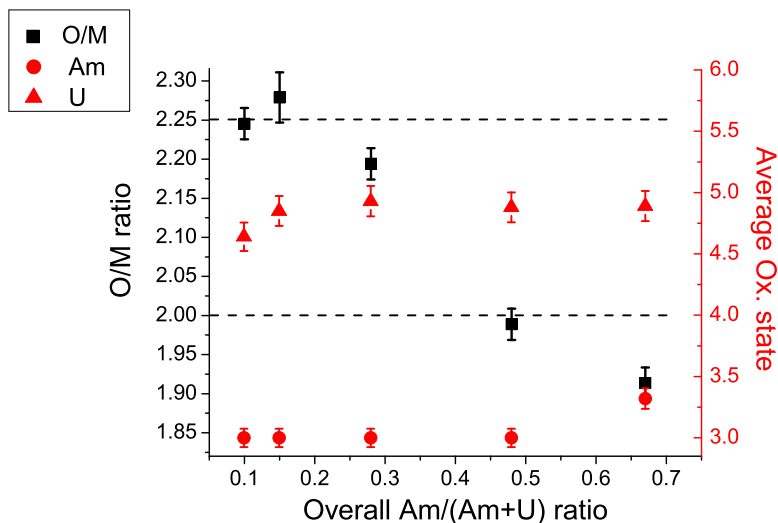


Figure 3: Compositions of the cubic phase of the oxidized samples as a function of the overall O/M ratio of the sample.

The obtained O/M ratios confirm the identification of the cubic structure of the *Am10ox*, *Am15ox* samples with the M₄O₉ phase. The O/M = 2.19 of the *Am30ox* sample is consistent with the oxidation of the MO_{2+x} phase, highlighted by the HT-XRD results shown in the first part.¹³ For the monophasic *Am50ox* sample, the O/M ratio is close to the stoichiometric

value. This value is consistent with the variation in the lattice parameter observed during the HT-XRD measurements, which did not indicate a substantial oxidation of the sample. For the *Am70ox* sample, it is hard to draw conclusions since the average oxidation of uranium could not be measured after the oxidation. However, considering the HT-XRD data and the americium behaviour (only slightly oxidized), one can suppose that the oxide was still hypo-stoichiometric, even after the thermal treatment in air.

3.2 EXAFS results

Am L_{III} and U L_{II} EXAFS spectra were collected at 15 K on the oxidized samples. The obtained EXAFS spectra and their Fourier transforms are reported in Fig. 4 and Fig. 5, for Am and U respectively (the *Am70ox* sample is not reported because of the problems in the preparation).

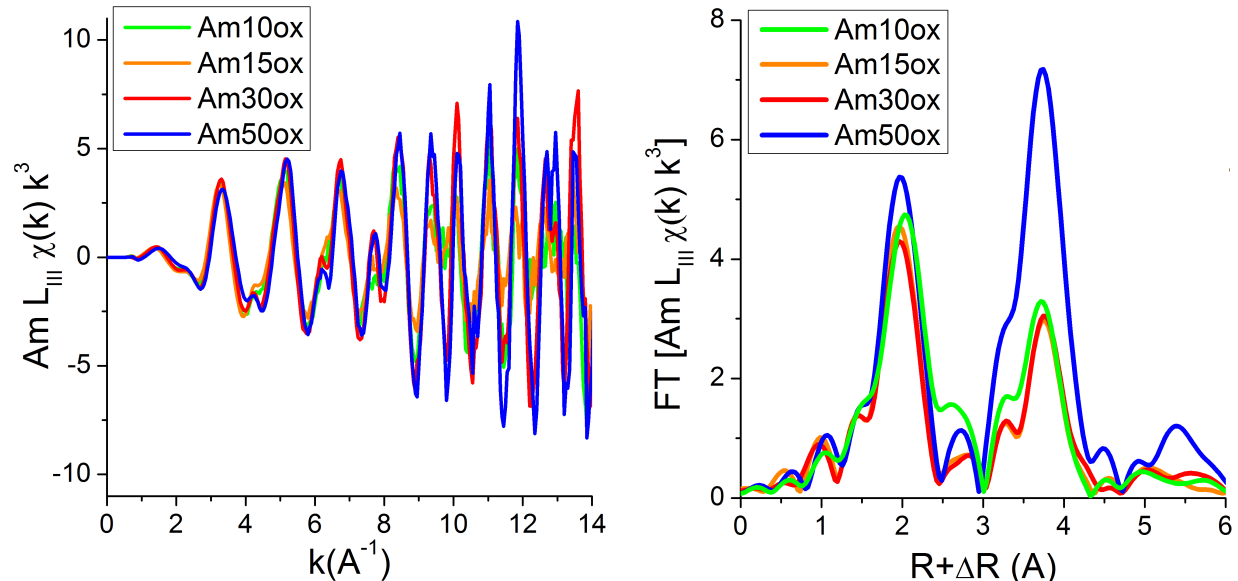


Figure 4: Experimental EXAFS spectra at the L_{III} edge of Am and their Fourier transforms of the oxidized samples. FT boundaries: 3.5-12 \AA^{-1} , $dk=2 \text{\AA}^{-1}$

Remarkable differences can be observed for both the Am L_{III} and U L_{II} EXAFS spectra between the different compositions.

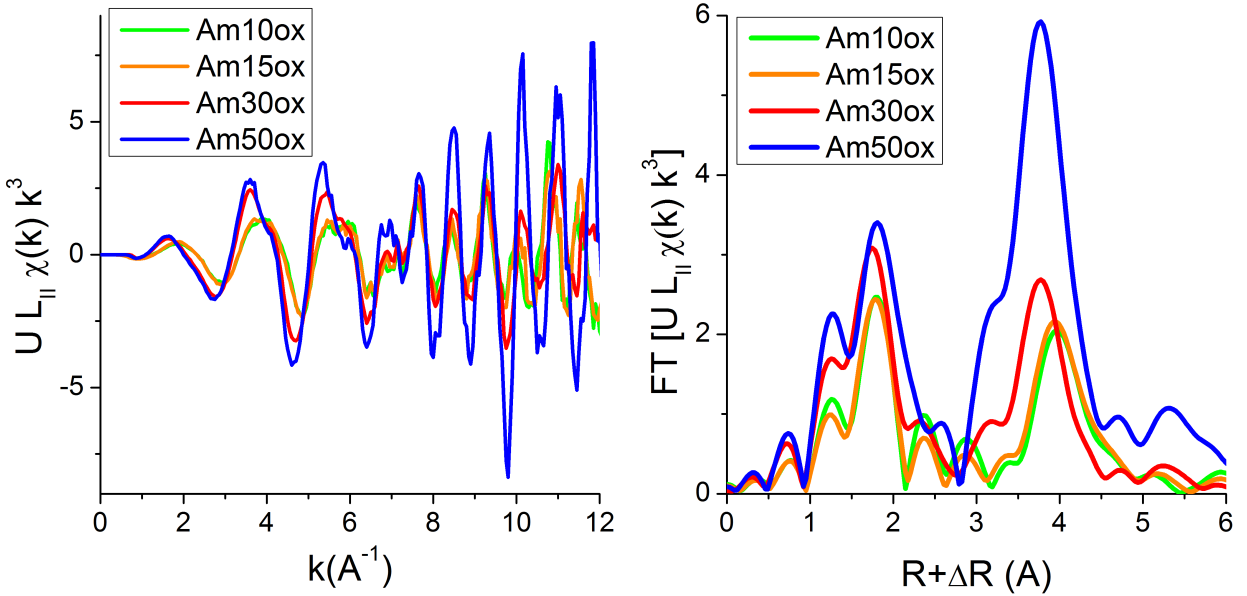


Figure 5: Experimental EXAFS spectra at the L_{II} edge of U and their Fourier transforms of the oxidized samples. FT boundaries: $3.5\text{-}11 \text{ \AA}^{-1}$, $dk = 2 \text{ \AA}^{-1}$

For the monophasic *Am50ox* sample, the EXAFS spectra present features similar to those of the corresponding as-sintered composition, which was previously reported by Epifano *et al.*⁸ In particular, the Fourier transform of the Am- L_3 EXAFS spectra exhibits two main peaks, around 1.9 \AA and 3.8 \AA respectively, which are characteristic of the fluorite structure. The first peak corresponds to the first cationic coordination shell in the fluorite environment, which is constituted by 8 oxygen neighbours; the second peak is mainly due to the contributions from the second coordination shell, constituted by twelve cations. Confirming these qualitative observations, the Am- L_3 EXAFS data are very well refined using a fluorite-type structural model, as shown in Figure 6.

For the U- L_2 edge EXAFS data, a clear broadening of the first peak of the Fourier transform can be observed. This broadening was previously observed for $U_{0.52}Am_{0.48}O_{1.97}$ (the oxide before the annealing in air)⁸ and it presents analogies with U_4O_9 .²² For this reason, as previously done for the as-sintered compound,⁸ a structural model based on the

β -U₄O₉ structure (F-43m), proposed by Cooper and Willis,²² was used for the refinement of the EXAFS data. In this structure, the cations and most of the O atoms are located at fluorite-type positions, but the fluorite-type oxygen sublattice (O_{fluo} in Table 5) shows a significant content of vacancies, whereas two additional interstitial positions are available for oxygen: the 48(h) (x = y = 0.617 and z = 0.5) and the 16(e) (x = y = z = 0.608) Wyckoff positions. However, since the 16(e) position has a very low occupancy (0.010), only the 48(h) interstitial oxygen atoms were included in the EXAFS model (O_{cubo} in Table 5). The main effect of including these cuboctahedral interstitials is the appearance of two additional U-O distances: one at about 2.20 Å and the other at about 2.87 Å, hence respectively shorter and longer than the U-O_{fluo} distance. A general good agreement between the fits and the data was obtained, as shown in Fig. 6.

The resulting structural parameters, listed in Tab. 5, are very similar to those previously obtained for the as-sintered oxide.⁸ More specifically, almost identical values, within the

Table 5: Parameters resulting from the refinement of the *Am50ox* EXAFS spectra.

Sample	Edge	Shell	R (Å)	N	$\sigma^2(\text{Å}^2)$	R-factor
U _{0.5} Am _{0.5} O ₂	Am-L _{III}	O1	2.426(5)	8.1(3)	0.0063(5)	0.009
		Am/U1	3.85(1)	12.1(5)	0.0042(4)	
		O2	4.47(1)	24(3)	0.014(3)	
	U-L _{II}	Am/U2	5.45(2)	6(2)	0.005(1)	0.011
		O _{cubo} 1	2.19(1)	1.7(5)	0.0073(5)	
		O _{fluo} 1	2.32(1)	5.4(5)	0.011(2)	
		O _{cubo} 2	2.82(1)	1.7(5)	0.012(2)	
		Am/U1	3.86(1)	12(1)	0.0045(5)	
	O _{fluo} 2	4.43(1)	25(3)	0.011(1)		

uncertainty limits, were obtained for the Am L₃ edge. Few differences were observed for the uranium local environment, consisting in slightly shorter U-O distances: for U-O_{fluo1}, a distance of 2.31(1) Å was here obtained, against 2.36(1) Å for the oxide before oxidation;⁸ similarly, 2.82(1) Å was here obtained for U-O_{cubo2}, against 2.87(1) Å in the previous work.⁸ This is consistent with the higher average oxidation state of uranium highlighted by the XANES and it confirms the slight increase in the O/M ratio from 1.97(1) to 1.99(2).

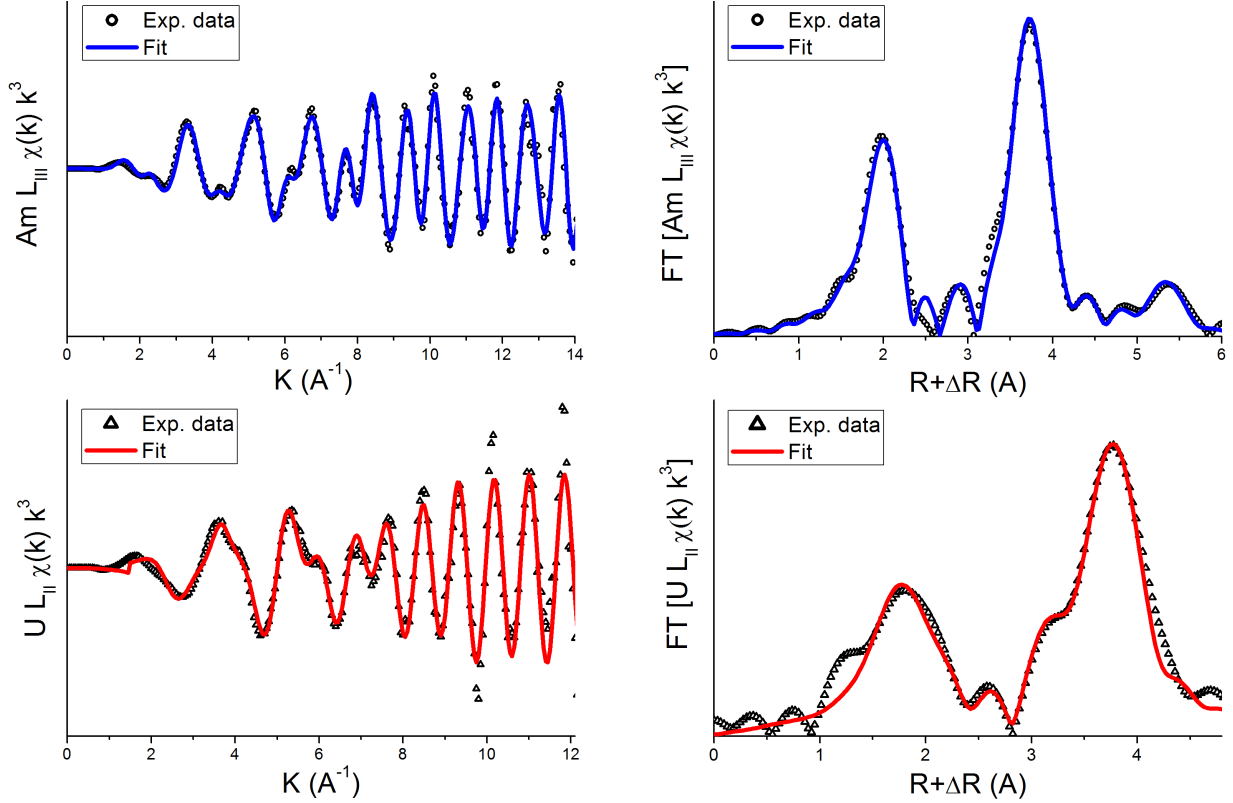


Figure 6: Am L₃ and U L₂ EXAFS spectra and Fourier transforms of the *Am50ox* sample. FT boundaries: 3.5-13.5 Å⁻¹, dk = 2 Å⁻¹ for Am L₃; 3.5-11.2 Å⁻¹, dk= 2 Å⁻¹ for U L₂.

The EXAFS spectra of the *Am10ox*, *Am15ox*, *Am30ox* could not be fitted by a theoretical model, since the presence of two complex structures (M₃O₈ and a cubic oxidized phase) would have required the refinement of too many parameters.

The U-L_{II} EXAFS spectra could be fitted by linear combination of the U₄O₉ and U₃O₈ references, achieving a reasonable agreement, as shown in Fig. 7. The results of the fits are summarized in Tab. 6. The M₄O₉/M₃O₈ phase proportion obtained for *Am10ox* is in very good agreement with the results obtained by the Rietveld refinement of the XRD data. For the *Am15ox* and *Am30ox* samples, the U₃O₈ contribution to the EXAFS fit is slightly higher than the amount of the M₃O₈ phase determined by XRD. This is consistent with the amount of americium in M₃O₈ being limited to a maximum value of 10 at.%. Indeed, this phase results enriched in uranium and, considering that the EXAFS provides information

only on the uranium environment, a higher M_3O_8 fraction is expected from the fit of these data.

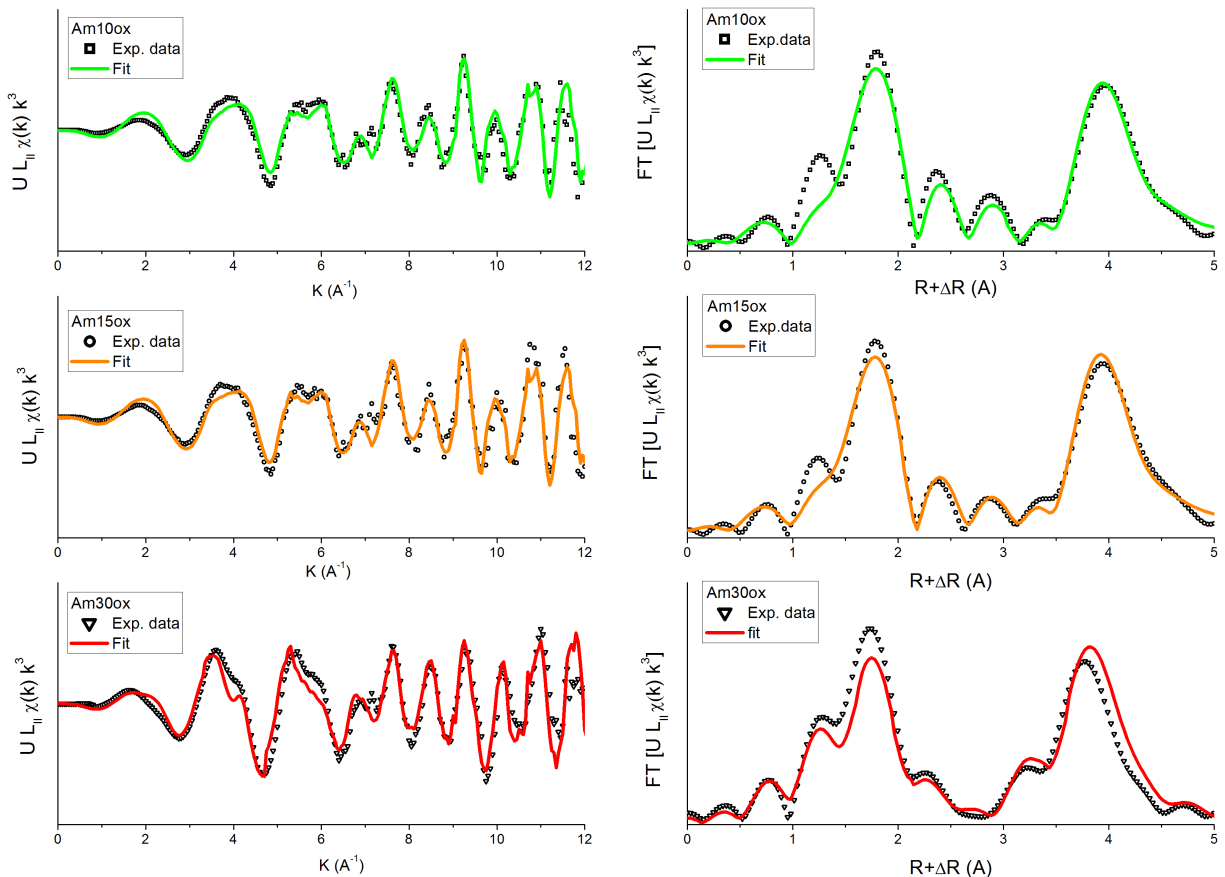


Figure 7: U L_2 EXAFS spectra and Fourier transforms of the *Am10ox*, *Am15ox* and *Am30ox* sample. FT boundaries: 3.5-11.5 \AA^{-1} , $dk = 2 \text{\AA}^{-1}$.

Table 6: Linear combination fits of the $\chi(k) \cdot k^3$ data.

Sample	Linear Combination Fit results		
	U_4O_9	U_3O_8	R-factor
Am10ox	0.23	0.77	0.1
Am15ox	0.31	0.69	0.09
Am30ox	0.82	0.18	0.12

The Am- L_{III} EXAFS spectra of the *Am10ox*, *Am15ox* and *Am30ox* samples, shown in Fig. 4, exhibit significant differences from the defect-free fluorite structure (see for comparison the *Am50ox* spectrum). For instance, in the relative k^3 -Fourier Transform, a decrease in the intensity of the second main peak (corresponding to the cationic shell) can be remarked. This

is due to the loss of the long range order around americium and it indicates a departure from the fluorite structure. The loss of the fluorite-type local environment, observed for the first time in U-Am mixed oxides, is consistent with americium incorporation in the oxygen-rich M_4O_9 and M_3O_8 phases.

4 Discussion

In this work, the composition of U-Am mixed oxides, after annealing in air at 1473 K, has been determined by combining XRD and XAS. Fundamental data on the O-rich domain of the U-Am-O phase diagram can be obtained from these results, assuming that: first, the thermal treatment was long enough to achieve equilibrium; second, the cooling was fast enough to quench the sample and maintain the composition. The first hypothesis relies on the HT-XRD results presented in another study,¹³ from which the samples here investigated originate. During the 4-hours dwell at 1473 K, the XRD patterns, acquired every 30 minutes, did not show any differences, indicating that the sample compositions were not evolving.¹³ Subsequently, during the cooling, XRD patterns were acquired every 100 K and the obtained lattice parameters decreased linearly, without discontinuities (see Annex). When a change in composition occurs, discontinuities are generally observed in the lattice parameters. For this reason, the hypothesis that the cooling was fast enough to preserve the equilibrium reached at 1473 K seems reasonable. Under these assumptions, data on the U-Am-O phase equilibria were obtained.

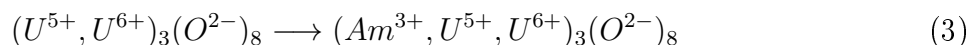
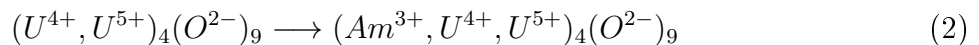
The accommodation of Am^{3+} in the M_4O_9 phase was observed for the first time. A small solubility of Am^{3+} ($Am/M \simeq 0.10$) in the M_3O_8 phase, previously proposed by Caisso *et al.*¹² for the hexagonal α' polymorph, was confirmed and it was extended also to the orthorhombic α structure. Fixing the Am/M ratio of the M_3O_8 phase to 10 mol.% for all the biphasic samples and combining the XRD and XANES data, the exact compositions can be proposed. These are summarized in Table 7 and represented on a isothermal section of the U-Am-O

phase diagram in Figure 8. Two tie-lines in the M_4O_9 - M_3O_8 , one tie line in the MO_{2+x} - M_3O_8 and two points in the $MO_{2\pm x}$ domain (the $Am/M = 0.67$ being uncertain, for the reasons previously explained) were obtained. Interestingly, the fluorite structure is preserved for $Am/(Am+U) \geq 0.48$, without the formation of hyper oxides. This is consistent with a recent result from Vigier *et al.*, who investigated by thermo-gravimetric analysis (TGA) the behaviour of a U-Am mixed oxide with $Am/M = 0.80$ (and some percent of Np and Pu impurities), in O_2 . Their results showed a mass intake for $438 \leq T \leq 650$ K, followed by a constant TGA signal up to 1273 K. After the annealing, the sample exhibited a single fluorite structure, in agreement with this work. Unfortunately, the O/M ratio of the sample was not measured (neither before nor after the TGA experiment) and hence the point cannot be added to our phase diagram.

Table 7: Obtained phase diagram points at 1473 K.

Overall composition		Chemical formula [mol.%]
Am/M	O/M	
0.1	2.48	$0.45 \cdot (U_{0.9}, Am_{0.1})_4O_9 + 0.55 \cdot (U_{0.9}, Am_{0.1})_3O_8$
0.15	2.37	$0.7 \cdot (U_{0.83}, Am_{0.17})_4O_9 + 0.3 \cdot (U_{0.9}, Am_{0.1})_3O_8$
0.28	2.20	$0.98 \cdot (U_{0.71}, Am_{0.29})O_{2.19} + 0.02 \cdot (U_{0.9}, Am_{0.1})_3O_8$
0.48	1.99	$(U_{0.52}, Am_{0.48})O_{1.99}$
0.67	≥ 1.91	$(U_{0.33}, Am_{0.67})O_{1.91+x}$

The phase diagram data here presented can be very useful in the frame of the development of a CALPHAD database for nuclear materials, such as the TAFID (Thermodynamics of Advanced nuclear Fuel International Database).²³ Guéneau *et al.* have reported a CALPHAD model for the U-O system, where the U_4O_9 and U_3O_8 phases were assessed within the compound energy formalism, using a two sublattice model.²⁴ According to the new results of this work, for the assessment of the U-Am-O system, these models should be extended as:



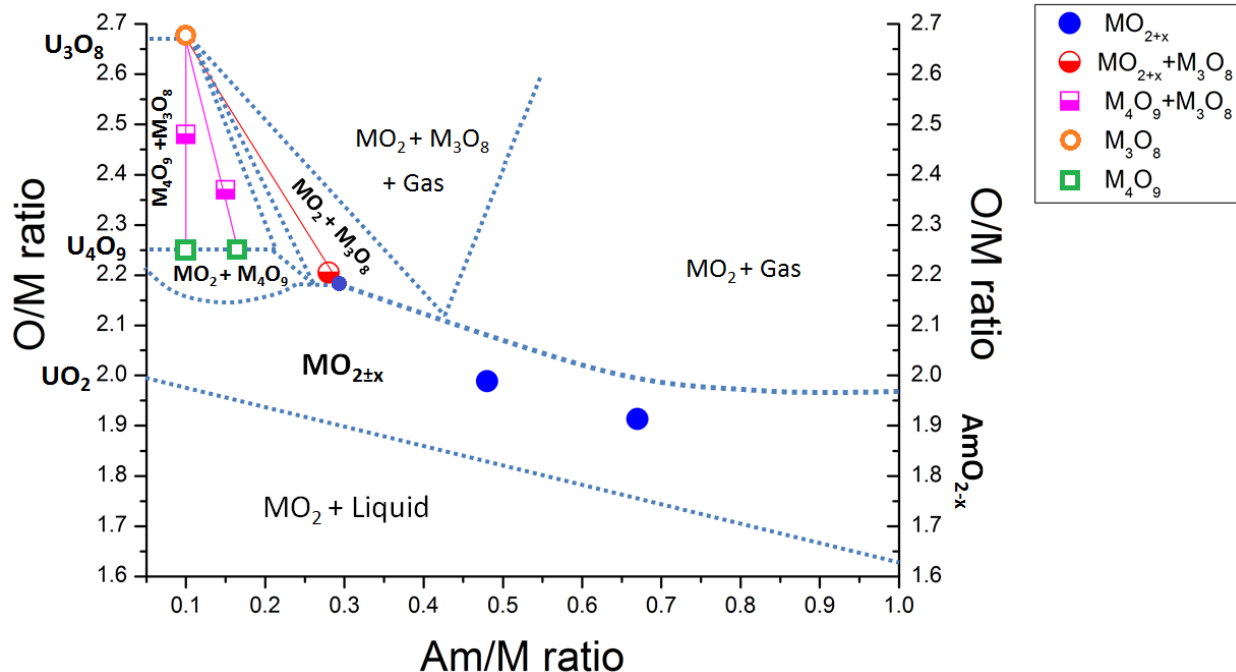


Figure 8: Possible iso-T section at 1470 K of the U-Am-O phase diagram and experimental points here obtained.

The two models are represented in Fig. 9, with the end members at the triangle vertexes and the theoretical stable solid solution represented by a red line. The models indicate that,

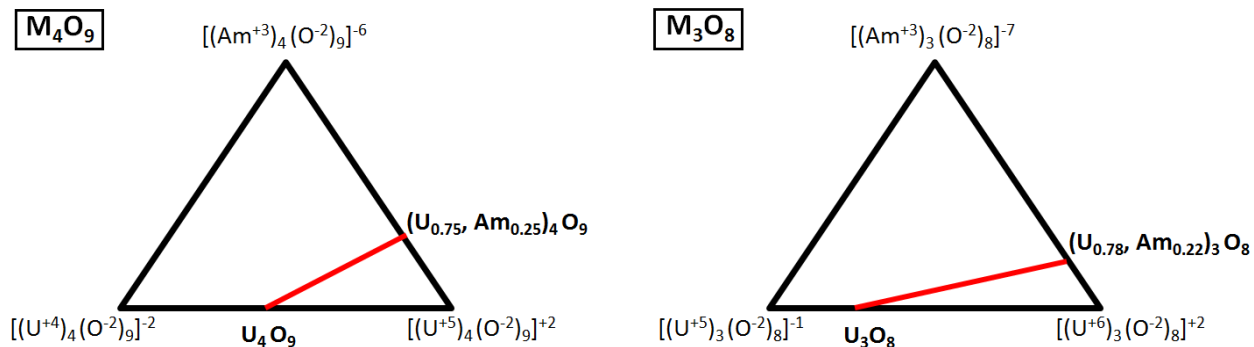


Figure 9: Schematic representation of the M_4O_9 and M_3O_8 CALPHAD models.

considering only trivalent americium, the maximum theoretical Am/M ratios in M_4O_9 and M_3O_8 are 0.25 and 0.22, respectively. They are likely even lower, especially for M_3O_8 , for which the solubility seems limited to $Am/M \leq 10$ at%. However, even if overestimated, the theoretical limits allow explaining the oxidation process exhibited by *Am30ox* during

the HT-XRD experiments and detailed in the first part of the work. For this oxide with $\text{Am}/(\text{Am}+\text{U}) = 0.28$, the oxidation proceeded by entering the $\text{MO}_{2+x}+\text{M}_3\text{O}_8$ domain for $T \gtrsim 1000$ K, without passing through the formation of M_4O_9 , as instead observed for *Am10ox* and *Am15ox*. At first, this was surprising since, in the binary U-O system, the $\text{UO}_{2+x}+\text{U}_3\text{O}_8$ equilibrium is possible only for $T > 1400$ K. This peculiarity is explained by the presence of americium in the trivalent state, which limits the Am/M ratios in M_4O_9 and M_3O_8 to 0.25 and 0.22. Both the values are lower than the overall Am/M ratio of the *Am30ox* sample (0.28). This implies that the establishment of the 2-phase $\text{M}_4\text{O}_9+\text{M}_3\text{O}_8$ equilibrium is not thermodynamically possible. Therefore, it is understandable that a high americium content ($\text{Am}/\text{M} \gtrsim 0.25$) induces a stabilization of the $\text{MO}_{2+x}+\text{M}_3\text{O}_8$ domain, which extends over a larger temperature range than that in the U-O system.

5 Conclusions and perspectives

The phase equilibria of the U-Am-O system, in the $\text{MO}_{2\pm x}-\text{M}_4\text{O}_9-\text{M}_3\text{O}_8$ domain, at 1473 K, were here investigated. Samples with $0.10 \leq \text{Am}/(\text{Am}+\text{U}) \leq 0.67$ were oxidized under air, during an *in situ* high-temperature XRD experiment, with a plateau temperature at 1473 K. The quenched samples were then characterized by X-ray Absorption Spectroscopy. The combination of these results and the previous XRD data allowed obtaining the compositions of the oxidized samples. Five phase diagram points at 1473 K were hence obtained: two tie-lines in the $\text{M}_4\text{O}_9-\text{M}_3\text{O}_8$, for $\text{Am}/(\text{Am}+\text{U}) = 0.10$ and 0.15, one tie-line in the $\text{MO}_{2+x}-\text{M}_3\text{O}_8$ domain, for $\text{Am}/(\text{Am}+\text{U}) = 0.28$, and two points in the single-phase $\text{MO}_{2\pm x}$ domain, for $\text{Am}/(\text{Am}+\text{U}) = 0.48$ and 0.67.

On the basis of these results, it can be concluded that americium is slightly soluble in both M_4O_9 and M_3O_8 . Quite surprisingly, the XANES data show that, despite the $\text{O}/\text{M} > 2.0$, the americium present in these structures is still trivalent. No tetravalent americium has been detected in M_4O_9 nor M_3O_8 . However, even if surprising, this is consistent with

several previous works, which showed a high stability of trivalent americium in U-Am mixed oxides.^{3,5,8} The maximum americium solubility in M_3O_8 has been determined at 10 at.%, while up to 15 at.% of americium was observed in the M_4O_9 phase (in the *Am15ox* sample). For the latter phase, the maximum value was not determined but, considering the trivalent state of americium, the solubility in M_4O_9 must be ≤ 0.25 at.%. Indeed, this is confirmed by the results obtained on the oxide with a total americium content equal to $Am/(Am+U) = 0.28$: in this case, the M_4O_9 was not formed and the $MO_{2\pm x}$ solid solution was in equilibrium with the M_3O_8 phase. This two-phase domain was observed starting from 1000 K, while in the U-O system it only exists for temperatures above 1400 K. Therefore, the americium addition extends the existence of the $MO_{2\pm x}+M_3O_8$ domain.

In conclusion, this work has provided new phase diagram points for the U-Am-O system and it has allowed determining the solubility of americium in the M_3O_8 and M_4O_9 oxides, together with its oxidation state in these structures. These data will be precious for the future development of a CALPHAD model of the U-Am-O system.

A Annex: Preparation of the samples by HT-XRD

The oxidized samples investigated in this work come from a previous study by high-temperature XRD. The lattice parameters of the cubic phases, shown in Fig. 10, exhibited a linear decrease during the cooling, without abrupt changes.

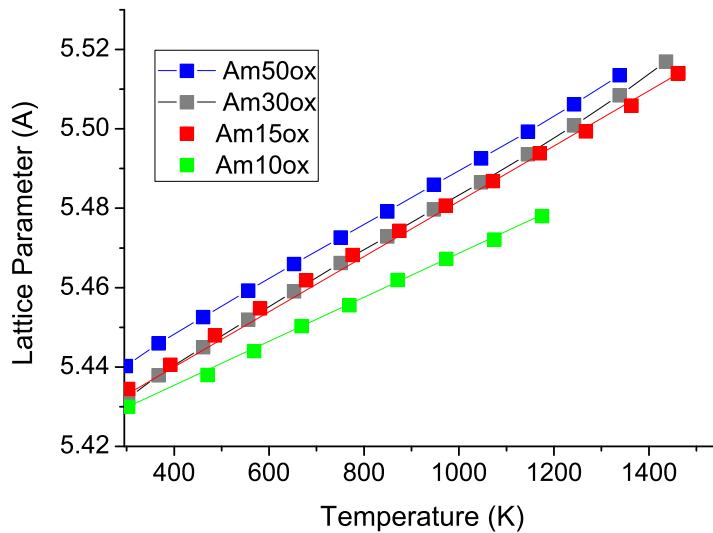


Figure 10: Lattice parameters of the cubic phases (M_4O_9 and $MO_{2\pm x}$) during the cooling in the HT-XRD. (Uncertainties in the symbol sizes).

References

- (1) D'Agata, E.; Hania, P. R.; Bejaoui, S.; Sciolla, C.; Wyatt, T.; Hannink, M. H. C.; Herlet, N.; Jankowiak, A.; Klaassen, F. C.; Lapetite, J. M.; Boomstra, D. A.; Philip, M.; Delage, F. The results of the irradiation experiment MARIOS on americium transmutation. *Annals of Nuclear Energy* **2013**, *62*, 40–49.
- (2) Prieur, D.; Jankowiak, A.; Delahaye, T.; Herlet, N.; Dehaut, P.; Blanchart, P. Fabrication and characterisation of $\text{U}_{0.85}\text{Am}_{0.15}\text{O}_{2-x}$ discs for MARIOS irradiation program. *Journal of Nuclear Materials* **2011**, *414*, 503–507.
- (3) Lebreton, F.; Horlait, D.; Caraballo, R.; Martin, P. M.; Scheinost, A. C.; Rossberg, A.; Jégou, C.; Delahaye, T. Peculiar Behavior of $(\text{U},\text{Am})\text{O}_{2-x}$ Compounds for High Americium Contents Evidenced by XRD, XAS, and Raman Spectroscopy. *Inorg. Chem.* **2015**, *54*, 9749–9760.
- (4) Prieur, D.; Martin, P. M.; Jankowiak, A.; Gavilan, E.; Scheinost, A. C.; Herlet, N.; Dehaut, P.; Blanchart, P. Local Structure and Charge Distribution in Mixed Uranium–Americium Oxides: Effects of Oxygen Potential and Am Content. *Inorg. Chem.* **2011**, *50*, 12437–12445.
- (5) Prieur, D.; Martin, P.; Lebreton, F.; Delahaye, T.; Banerjee, D.; Scheinost, A. C.; Jankowiak, A. Accommodation of multivalent cations in fluorite-type solid solutions: Case of Am-bearing UO_2 . *Journal of Nuclear Materials* **2013**, *434*, 7–16.
- (6) Prieur, D.; Lebreton, F.; Caisso, M.; Martin, P. M.; Scheinost, A. C.; Delahaye, T.; Manara, D. Melting behaviour of americium-doped uranium dioxide. *The Journal of Chemical Thermodynamics* **2016**, *97*, 244–252.
- (7) Epifano, E.; Beneš, O.; Vălu, O. S.; Zappey, J.; Lebreton, F.; Martin, P. M.; Guéneau, C.; Konings, R. J. M. High temperature heat capacity of $(\text{U}, \text{Am})\text{O}_{2\pm x}$. *Journal of Nuclear Materials* **2017**, *494*, 95–102.

- (8) Epifano, E.; Naji, M.; Manara, D.; Scheinost, A. C.; Hennig, C.; Lechelle, J.; Konings, R. J. M.; Guéneau, C.; Prieur, D.; Vitova, T.; Dardenne, K.; Rothe, J.; Martin, P. M. Extreme multi-valence states in mixed actinide oxides. *Communications Chemistry* **2019**, *2*, 59.
- (9) Epifano, E.; Prieur, D.; Martin, P. M.; Guéneau, C.; Dardenne, K.; Rothe, J.; Vitova, T.; Dieste, O.; Wiss, T.; Konings, R. J. M.; Manara, D. Melting behaviour of uranium-ameridium mixed oxides under different atmospheres. *The Journal of Chemical Thermodynamics* **2020**, *140*, 105896.
- (10) Vigier, J.-F.; Freis, D.; Pöml, P.; Prieur, D.; Lajarge, P.; Gardeur, S.; Guiot, A.; Bouëxière, D.; Konings, R. J. M. Optimization of Uranium-Doped Americium Oxide Synthesis for Space Application. *Inorganic Chemistry* **2018**, *57*, 4317–4327.
- (11) Bartscher, W.; Sari, C. A thermodynamic study of the uranium-ameridium oxide $\text{U}_{0.5}\text{Am}_{0.5}\text{O}_2$. *Journal of Nuclear Materials* **1983**, *118*, 220–223.
- (12) Caisso, M.; Roussel, P.; Den Auwer, C.; Picart, S.; Hennig, C.; Scheinost, A. C.; Delahaye, T.; Ayrat, A. Evidence of Trivalent Am Substitution into U_3O_8 . *Inorg. Chem.* **2016**, *55*, 10438–10444.
- (13) Epifano, E.; Vauchy, R.; Lebreton, F.; Joly, A.; Guéneau, C.; Martin, P. M. Behaviour of $(\text{U},\text{Am})\text{O}_2$ in oxidizing conditions: a high-temperature XRD study. *submitted to Journal of Nuclear Materials*
- (14) Delahaye, T.; Lebreton, F.; Horlait, D.; Herlet, N.; Dehaut, P. Application of the UMACS process to highly dense $\text{U}_{1-x}\text{Am}_x\text{O}_2$ MABB fuel fabrication for the DIAMINO irradiation. *Journal of Nuclear Materials* **2013**, *432*, 305–312.
- (15) Lebreton, F.; Horlait, D.; Delahaye, T.; Blanchart, P. Fabrication and characterization of $\text{U}_{1-x}\text{Am}_x\text{O}_2$ compounds with high americium contents ($x = 0.3, 0.4$ and 0.5). *Journal of Nuclear Materials* **2013**, *439*, 99–102.

- (16) Horlait, D.; Lebreton, F.; Roussel, P.; Delahaye, T. XRD Monitoring of alpha Self-Irradiation in Uranium–Americium Mixed Oxides. *Inorganic Chemistry* **2013**, *52*, 14196–14204.
- (17) Ravel, B.; Newville, M. ATHENA, ARTEMIS, HEPHAESTUS: data analysis for X-ray absorption spectroscopy using IFEFFIT. *J Synchrotron Radiat* **2005**, *12*, 537–541.
- (18) Arab-Chapelet, B.; Martin, P. M.; Costenoble, S.; Delahaye, T.; Scheinost, A. C.; Grandjean, S.; Abraham, F. Multiscale structural characterizations of mixed U(IV)–An(III) oxalates (An(III) = Pu or Am) combining XAS and XRD measurements. *Dalton Transactions* **2016**, *45*, 6909–6919.
- (19) Prieur, D.; Vigier, J.-F.; Wiss, T.; Janssen, A.; Rothe, J.; Cambriani, A.; Somers, J. Structural investigation of self-irradiation damaged AmO₂. *Journal of Solid State Chemistry* **2014**, *212*, 7–12.
- (20) Kvashnina, K. O.; Butorin, S. M.; Martin, P.; Glatzel, P. Chemical State of Complex Uranium Oxides. *Phys. Rev. Lett.* **2013**, *111*, 253002.
- (21) Rehr, J. J.; Ankudinov, A.; Zabinsky, S. I. New developments in NEXAFS/EXAFS theory. *Catalysis Today* **1998**, *39*, 263–269.
- (22) Cooper, R. I.; Willis, B. T. M. Refinement of the structure of beta-U₄O₉. *Acta Cryst A, Acta Cryst Sect A, Acta Crystallogr A, Acta Crystallogr Sect A, Acta Crystallogr A Found Crystallogr, Acta Crystallogr Sect A Found Crystallogr* **2004**, *60*, 322–325.
- (23) Geiger, E.; Guéneau, C.; Pontillon, Y.; Corcoran, E. C. Modelling nuclear fuel behaviour with TAF-ID: Calculations on the VERDON-1 experiment, representative of a nuclear severe accident. *Journal of Nuclear Materials* **2019**, *522*, 294–310.
- (24) Guéneau, C.; Dupin, N.; Sundman, B.; Martial, C.; Dumas, J.-C.; Gossé, S.; Chatain, S.; Bruycker, F. D.; Manara, D.; Konings, R. J. M. Thermodynamic modelling

of advanced oxide and carbide nuclear fuels: Description of the U–Pu–O–C systems.
Journal of Nuclear Materials **2011**, *419*, 145–167.